## Supplementary Materials and Methods

### (I) Supplementary Methods

### Whole mount immunostaining

E12.5 embryonic hearts were dissected out and fixed in 4% paraformaldehyde for 3 hours, washed in PBT (PBS with 0.1% Tween), and incubated in blocking solution (5% serum, PBS, 0.5% Triton X-100) for 2 hours. Primary antibodies incubation was at 4˚C overnight in blocking solution. Hearts were washed with PBT and incubated with secondary antibodies at 4˚C overnight in blocking solution. Hearts were washed with PBT, fixed again in 4% paraformaldehyde for 2 hours, and then washed with PBT. Images were captured on Leica MZFLIII Microscope and antibodies used are listed in Table S8.

### Calcium transients and electrophysiology

Cardiomyocytes isolated from E11.5 embryos were plated onto laminin-coated coverslips (#1, Warner Instruments). After visible beating was confirmed, the myocytes were loaded with the $Ca^{2+}$-sensitive fluorescent indicator Fluo-4. Each whole coverslip was exposed to the cell membrane-permeant Fluo-4 AM, using a 1:10 mixture of the indicator (dissolved in dry dimethyl sulfoxide at 5 mM) plus Powerload concentrate (Life Technologies). This mixture was diluted 100-fold into extracellular Tyrode's solution and substituted for culture medium in dishes containing coverslips (final indicator concentration, 5 μM). Cells were loaded with indicator for 20 min at room temperature and placed in fresh extracellular solution for a further 20 min to allow for de-esterification, before recordings were taken. To commence experiments, a coverslip of indicator-loaded myocytes was placed in a superfusion bath (RC26-GLP, Warner Instruments) on a Nikon TiS inverted microscope equipped with a microfluorometer (IonOptix). The bathing solutions were warmed to 30°C with a superfusion system and heated perfusion pencil (AutoMate Scientific). The myocytes were superfused at a constant flow (DN series syringes, Warner Instruments) with modified Tyrode's extracellular solution containing (mM): NaCl 137, NaHEPES 10, dextrose 10, KCl 5, $CaCl_2$ 2, and

$MgCl_2$ 1, set to pH 7.4 with NaOH. Single, spontaneously contracting myocytes and small clusters (5 or fewer cells) were selected for study.

Fluo-4 fluorescence transients were recorded with a standard filter set with excitation centered on 480 nm and emission centered on 535 nm (#49011, Chroma Technology, Bellows Falls, VT). Fluorescence was obtained from contracting cells plus a cell-free border using a cell-framing adaptor (IonOptix). Between sampling periods, the excitation light was blocked with a shutter (Vincent Associates). $Ca^{2+}$-sensitive fluorescence signals were low-pass filtered at 2 kHz and digitized at 5 kHz for 30 s per data file. Mean durations for $[Ca^{2+}]_i$ transients were calculated by measuring up-to 40 individual responses per data file (depending on the spontaneous beating rate), corresponding to the sampling of one cell or cluster representing the particular genotype. Multiple samples were combined to get an overall mean to be used for graph plotting. Fluorescence signals were corrected by subtracting the mean background emission (present after removing the cell(s) from the field of view) from all data files, and changes in fluorescence amplitudes were expressed relative to the mean diastolic level attained between spontaneous beats (i.e. $F/F_o$). Changes in this relative fluorescence were considered to reflect underlying changes in intracellular $Ca^{2+}$ concentration. In a small number of additional experiments, Fluo-4 loaded cells were subjected to amphotericin B-perforated patch clamp (Spencer et al., 2014). Briefly, patch electrodes of approximately 2-4 MΩ (WPI) were tip-filled by dipping (for 20 s) in an intracellular solution containing (mM): KCl 120, NaHEPES 20, MgATP 10, $K_2$EGTA 5, $MgCl_2$ 2, adjusted to pH 7.1 with KOH, and then back filled with the same solution including amphotericin B (240 µg/ml). The action potentials associated with spontaneous $[Ca^{2+}]_i$ transients, were recorded (at 5 kHz as above) in current clamp mode with zero applied current, and were corrected for a –5.6 mV liquid junction potential. Unless stated otherwise, all reagents were from Sigma-Aldrich.

**Chromatin immunoprecipitation (ChIP)**

90 *Tnnt2::Cre;Kmt2d*$^{fl/fl}$ hearts and 90 *Tnnt2::Cre;Kmt2d*$^{fl/+}$ control hearts (from littermates) were collected at embryonic day 11.5. Formaldehyde was added to a final concentration of 1% to generate DNA-protein crosslinks for 10 minutes at room temperature, then quenched by adding glycine to a final concentration of 125mM. Hearts were pelleted at 430g at 4C for 5 minutes and washed twice in 10mL of ice-cold PBS. Hearts were then resuspended in 3mL of ice-cold cell lysis buffer (5mM PIPES, pH 8.0; 85mM KCl; 1.0% (v/v) NP- 40; 1x protease inhibitor cocktail) and incubated on ice for 15 minutes. Next, hearts were homogenized on ice using 20 strokes on a Dounce tissue grinder (Sigma-Aldrich). Homogenate was pelleted at 430g at 4C for 5 minutes, then resuspended in ice-cold nuclei lysis buffer (50mM Tris-Cl, pH 8.0; 10mM EDTA, pH 8.0; 1% (w/v) SDS; 1x protease inhibitor cocktail). Samples were incubated in nuclei lysis buffer for 30 minutes on ice and sonicated using a Bioruptor Standard (Diagenode) (6x5min cycles, 30s on/30s off, 4C) to shear chromatin into 200- 600bp fragments. Samples were pelleted for 10 minutes at 20,800xg at 4C and supernatants were diluted 1:5 with IP dilution buffer (50mM Tris-Cl, pH 7.4; 150mM NaCl, 1mM EDTA, pH 8.0; 1% (v/v) NP-40; 0.25% (w/v) sodium deoxycholate; 1x protease inhibitor cocktail). 3 ug of anti-H3K4me1 antibody, 3 ug of anti-H3K4me2 antibody, or 3 ug of anti-H3K4me3 antibody (listed in Table S8) were added to 3 control samples and 3 mutant samples (3 biological replicates per genotype per antibody). Samples were incubated overnight at 4˚C.

40uL of Protein G Dynabead (Life Technologies) suspension was added to each sample, incubated for 2 hours, then washed twice with IP wash buffer 1 (IP dilution buffer without protease inhibitors), twice with IP wash buffer 2 (100mM Tris-Cl, pH 9.0; 500mM LiCl; 1% (v/v) NP-40; 1% (w/v) sodium deoxycholate), and with IP wash buffer 3 (100mM Tris-Cl, pH 9.0; 500mM LiCl; 150mM NaCl; 1% (v/v) NP-40; 1% (w/v) sodium deoxycholate). Immunoprecipitated material was eluted by incubating at 65C for 30 minutes with shaking in 100uL of ChIP elution buffer (50mM NaHCO3, 1% (w/v) SDS). NaCl was added to each eluted

sample to a final concentration of 0.54M, and crosslinks were reversed by overnight incubation at 67˚C. Samples were treated with 10ug of RNase A for 30 minutes at 37˚C, and DNA was precipitated from each sample by adding 1.8x the sample volume of AMPure XP magnetic bead suspension (Beckman Coulter). Beads were washed 2x with 80% ethanol, dried, and beads were resuspended in 20uL water to elute DNA. Prepared libraries (Kapa Biosystems) were sequenced in 1x50bp mode on Illumina HiSeq 2500.

**ChIP-Exo**

For each replicate, $5x10^7$ cardiac myocytes were derived from E14 mouse embryonic stem cells via directed differentiation as previously described (Wamstad et al., 2012). Cells were pelleted, washed and resuspended in PBS. Disuccinimidyl glutarate (DSG), a long-range crosslinking agent, was added to a final concentration of 2mM and incubated for 45 minutes. Cells were pelleted, washed and resuspended in PBS containing 1% (v/v) formaldehyde for 15 minutes at room temperature. Formaldehyde crosslinking was quenched by adding glycine to a final concentration of 125mM and incubating for 10 minutes. Cells were then washed 3 times with ice-cold PBS, pelleted and flash frozen. To complete ChIP-exo, frozen cells were thawed on ice; lysis, homogenization, sonication, and immunoprecipitation were performed in the same fashion as they were for ChIP-Seq. We used an anti-KMT2D antibody provided by Kai Ge (NIH) with 8 ug per replicate (Lee et al., 2013). Following immunoprecipitation, ChIP-exo was performed as previously described (Serandour et al., 2013). Briefly, prior to the elution of immunoprecipitated DNA-containing complexes from the Protein G beads, DNA was polished and ligated with the Illumina P7 adapter. Nicks were then repaired, followed by exonuclease digestion. Following digestion, immunoprecipitated complexes were eluted from the beads and crosslinks were reversed. DNA was isolated from the eluate and denatured. Double-stranded DNA was generated from each single strand using a primer which anneals to the P7 adapter sequence. The resulting fragments were ligated with P5 adapter, followed by amplification via PCR with indexed primers. The

resulting DNA libraries were gel-purified and sequenced on an Illumina HiSeq 4000 to generate 50bp single-end reads with >100 million reads per sample.

**ChIP-Seq and ChIP-Exo analysis**

Sequencing reads were de-multiplexed using CASAVA version 1.8.2. Reads are trimmed using the Fastq-mcf program (http://code.google.com/p/ea-utils). Filtered reads are analyzed using the Fastqc program (Babraham Bioinformatics, Cambridge, United Kingdom). Reads were then aligned to the mm9 genome assembly using bowtie2 (Langmead and Salzberg, 2012) and filtered to retain only reads with a mapq score greater than or equal to 30 using SAMtools version 1.2 (Li et al., 2009). For tag calling, bam2bed is used to convert bam files into bed files, and the genome-wide shift between + and – strand tags is calculated in a manner adapted from the Kundaje method (Neph et al., 2012). The mm9 genome assembly was then split into 20bp bins, and tag density is defined as the number of tags that map to within 75 bp of each genomic bin (Landt et al., 2012). For ChIP-Seq, the same calculation was performed for each sample's associated input, and tag densities were normalized to input as follows:
tagDensity = #binsInGenome * ((#tags/#totalTags) - (#inputTags/#totalInputTags))

Publicly available Illumina sequencing data from H3K4me1 and H3K4me3 ChIP-seq experiments using both mouse embryonic stem cells and cardiac myocytes generated via directed differentiation (Wamstad et al., 2012) was filtered and aligned to the mm9 genome assembly in an identical manner to that described for the H3K4me1 and H3K4me3 ChIP-seq experiments we performed using E11.5 hearts. The Spearman correlation between the aligned reads from each experiment was then determined using bamCorrelate, part of the deepTools package (Ramírez et al., 2014). This tool allows for the comparison of ChIP-Seq experiments prior to any further manipulation of the data, such as read density smoothing or peak calling.

For ChIP-Exo, no input chromatin was provided and the tag densities are normalized as follows (Landt et al., 2012):
tagDensityOfGenomicBin = #tagsAtBin * #binsInEntireGenome / #totalTagsInDataset
To minimize false positives and false negatives, bins representing greater than 4.9-fold enrichment over input (tag density score ≥ 30) are accepted for ChIP-Seq and and bins representing greater than 6.6-fold enrichment over background (tag density score ≥ 100) are accepted for ChIP-Exo. Enriched bins are merged together throughout the genome and merged bins representing signal peaks spanning multiple genomic bins are retained. For ChIP-Seq, a total of 358,833 peaks were identified. To compare peak scores and perform differential enrichment, peaks are annotated with total tag density within peak regions. For ChIP-Exo, KMT2D binding events were defined by peaks present in 2 out of 3 replicates within 500 bp of each other. Genomic regions were associated with genes using GREAT (Mclean et al., 2010), with gene regulatory domain defined as proximal for 5 kb upstream and 1 kb upstream, distal for up to 100 kb in both directions to the nearest gene's basal domain.

## (II) Supplementary Figures

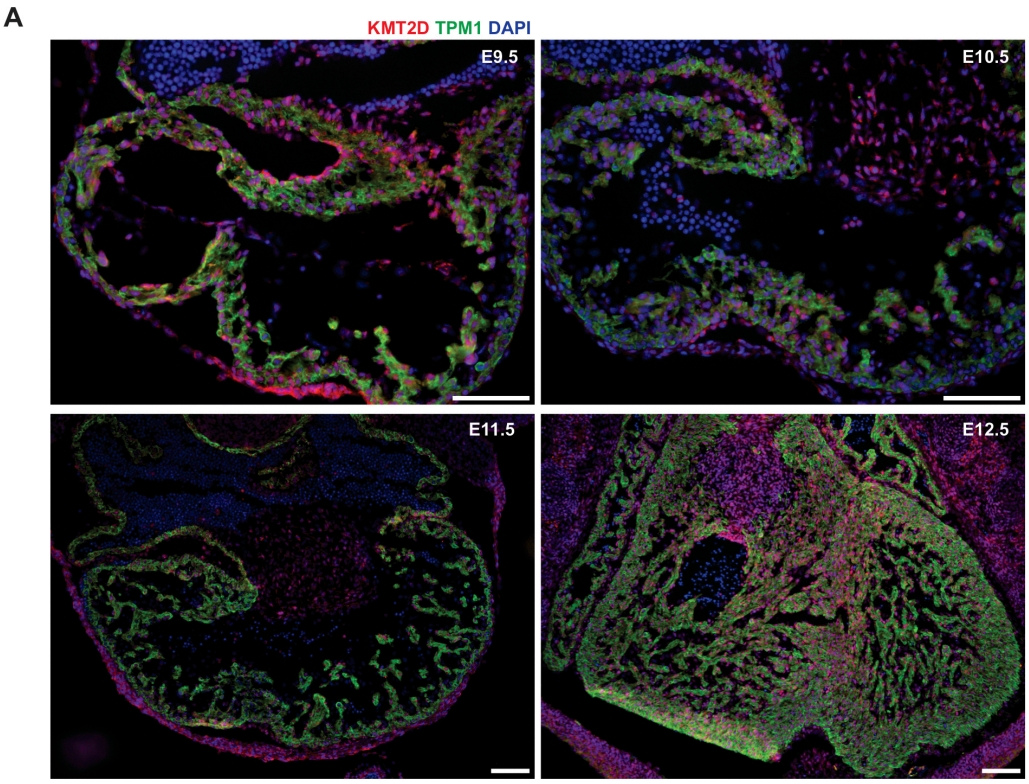


**Fig. S1. KMT2D is expressed broadly in the developing heart.**

(A) Immunostaining of E9.5, E10.5, E11.5 and E12.5 embryonic hearts in four-chamber view sections show ubiquitous KMT2D expression (green). Nuclei (DAPI) is stained in blue and the myocardium (TPM1) is stained in red. Scale bar = 100 μm.

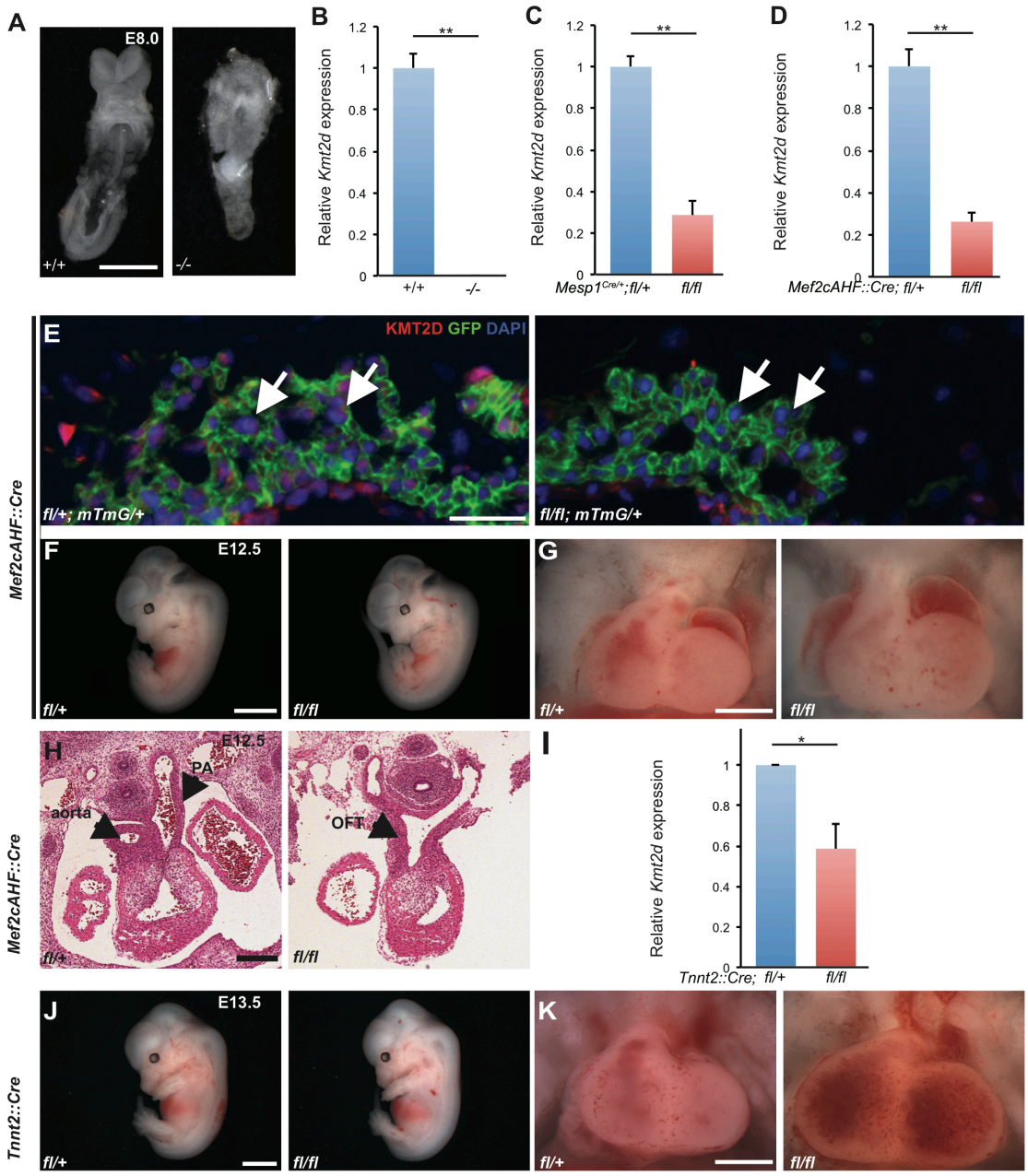


**Fig. S2. Deletion of *Kmt2d* in cardiac precursors and myocardium leads to loss of *Kmt2d* expression and minor changes in gross morphology.**

(A) Representative images of E8.0 control $Kmt2d^{+/+}$ and $Kmt2d^{\Delta/\Delta}$ embryos show severe developmental defects in mutants. Scale bar = 250 μm.

(B) qRT-PCR in E8.0 control $Kmt2d^{+/+}$ and $Kmt2d^{\Delta/\Delta}$ embryos show complete loss of *Kmt2d* transcript in mutants ($P$<0.01).

(C) qRT-PCR in E9.0 control *Mesp1*$^{Cre}$;*Kmt2d*$^{fl/+}$ and *Mesp1*$^{Cre}$;*Kmt2d*$^{fl/fl}$ whole hearts show 71.4% decrease in *Kmt2d* transcript levels in mutants ($P$<0.01).
(D) qRT-PCR in E11.5 control *Mef2cAHF::Cre;Kmt2d*$^{fl/+}$ and *Mef2cAHF::Cre;Kmt2d*$^{fl/fl}$ right ventricles and outflow tracts shows 73.8% decrease in *Kmt2d* transcript levels in mutants ($P$<0.01).
(E) E12.5 control and *Mef2cAHF::Cre;Kmt2d*$^{fl/fl}$ *Rosa*$^{mTmG/+}$ cardiac sections at four-chamber view are stained for KMT2D (red), GFP (green), DAPI (blue). Mutant interventricular septum shows loss of KMT2D expression in Cre-expressing GFP-positive cells. Scale bar = 100 μm.
(F) Representative images of E12.5 control and *Mef2cAHF::Cre;Kmt2d*$^{fl/fl}$ embryos show no obvious differences. Scale bar = 2 mm.
(G) Representative images of E12.5 control and *Mef2cAHF::Cre;Kmt2d*$^{fl/fl}$ hearts show no obvious differences. Scale bar = 500 μm.
(H) Representative images of E12.5 control and *Mef2cAHF::Cre;Kmt2d*$^{fl/fl}$ cardiac sections at four-chamber view show defects in outflow tract septation into pulmonary and aorta (arrows). Scale bar = 250 μm.
(I) qRT-PCR in E11.5 control and *Tnnt2::Cre;Kmt2d*$^{fl/fl}$ whole hearts shows 41.1% decrease in *Kmt2d* transcript levels ($P$<0.05). Incomplete loss is likely due to contribution of *Tnnt2::Cre*-negative non-myocyte population in hearts, including endocardium and cardiac fibroblasts.
(J) Representative images of E13.5 control and *Tnnt2::Cre;Kmt2d*$^{fl/fl}$ embryos show no obvious differences. Scale bar = 2 mm.
(K) Representative images of E13.5 control and *Tnnt2::Cre;Kmt2d*$^{fl/fl}$ hearts show no obvious differences. Scale bar = 250 μm.
PA, pulmonary artery; OFT, outflow tract. *$P$<0.05; **$P$< 0.01; error bars indicate SD.

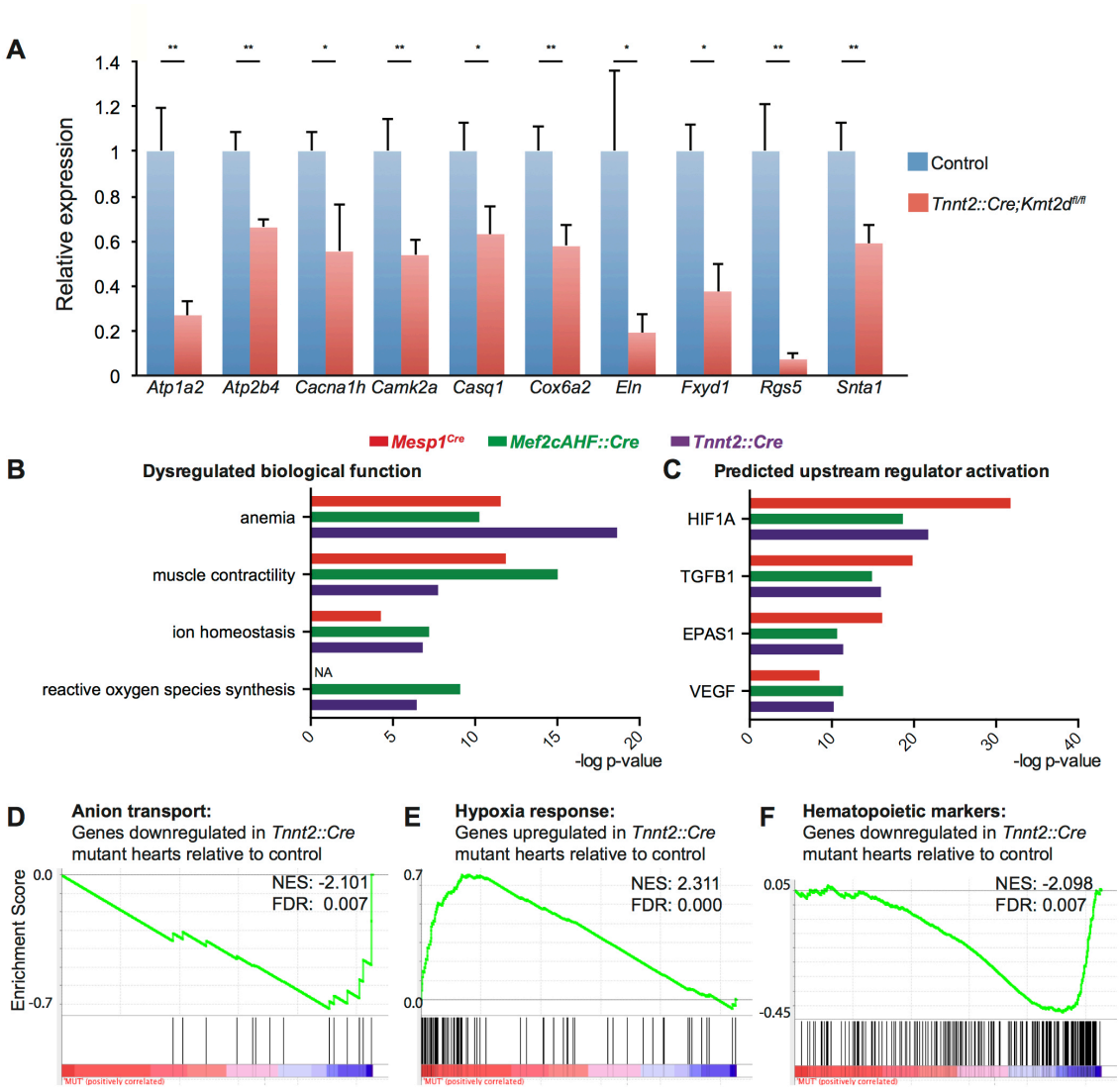


**Fig. S3. Deletion of *Kmt2d* in cardiac precursors and myocardium lead to downregulation of ion transport genes and upregulation of hypoxia response genes.**

(A) qRT-PCR in E11.5 control and *Tnnt2::Cre; Kmt2d*$^{fl/fl}$ embryos shows decreases in ion transport related genes (**P*< 0.05; ***P*< 0.01, error bars indicate SD).

(B) Ingenuity Pathway Analysis of differentially expressed genes in all three deletion genotypes shows that biological functions that were significantly dysregulated are associated with anemia, contractility of muscle, ion homeostasis and reactive oxygen species synthesis (*P*< 0.05).

(C) Ingenuity Pathway Analysis of differentially expressed genes in all three deletion genotypes shows that upstream regulators that were significantly predicted to be dysregulated are associated with hypoxia ($P$<0.05).
(D) GSEA shows a significant depletion of genes associated with anion transport in E11.5 *Tnnt2::Cre;Kmt2d*$^{fl/fl}$ mutants (FDR<0.01).
(E) GSEA shows a significant enrichment of genes associated with hypoxia response in E11.5 *Tnnt2::Cre;Kmt2d*$^{fl/fl}$ mutants (FDR<0.01).
(F) GSEA shows a significant depletion of genes associated with erythropoietic differentation in E11.5 *Tnnt2::Cre;Kmt2d*$^{fl/fl}$ mutants (FDR<0.01).

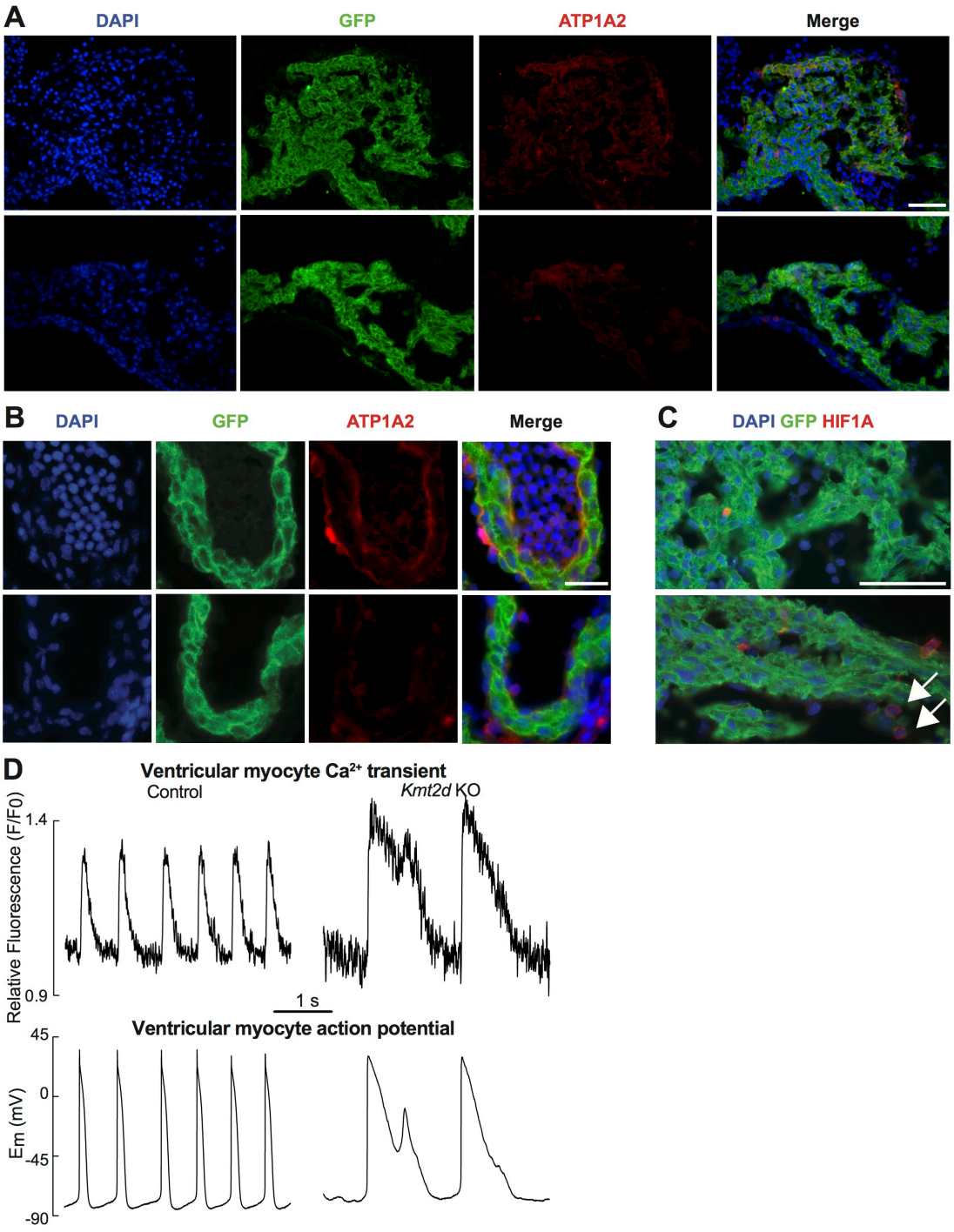


**Fig. S4. Deletion of *Kmt2d* in myocardium leads to decreased expression of ion transporter ATP1A2, increased expression of hypoxia response factor HIF1A and altered calcium handling in ventricular myocytes.**

(A) E11.5 control and *Tnnt2::Cre;Kmt2d*$^{fl/fl}$*; Rosa*$^{mTmG/+}$ cardiac sections at four-chamber view are stained for ATP1A2 (red), GFP (green) and DAPI (blue). Magnified image of interventricular septum shows loss of ATP1A2 expression in Cre-expressing GFP-positive cells. Scale bar = 50 μm.

(B) E11.5 control and *Tnnt2::Cre;Kmt2d*$^{fl/fl}$*; Rosa*$^{mTmG/+}$ cardiac sections at four-chamber view are stained for ATP1A2 (red), GFP (green) and DAPI (blue). Magnified image of left atria shows loss of ATP1A2 expression in Cre-expressing GFP-positive cells. Scale bar = 25 μm.

(C) E11.5 control and *Tnnt2::Cre;Kmt2d*$^{fl/fl}$*; Rosa*$^{mTmG/+}$ cardiac sections at four-chamber view are stained for HIF1A (red), GFP (green) and DAPI (blue). Magnified image of interventricular septum shows increase in HIF1A expression in GFP-negative cells (arrows). Scale bar = 50 μm.

(D) Fluo-4 fluorescence recordings (upper panel) and traces of action potentials (lower panel, $E_m$: membrane potential) from control and Tnnt2::Cre;*Kmt2d*$^{fl/fl}$ (*Kmt2d* KO) ventricular myocytes isolated at E11.5. Note the reduced action potential frequency, prolongation and secondary depolarization exhibited by the mutant cell, indicative of electrophysiological abnormality. Early after depolarizations (EADs) are observed in 3% of controls and 13% of *Kmt2d* KO ventricular myocytes.

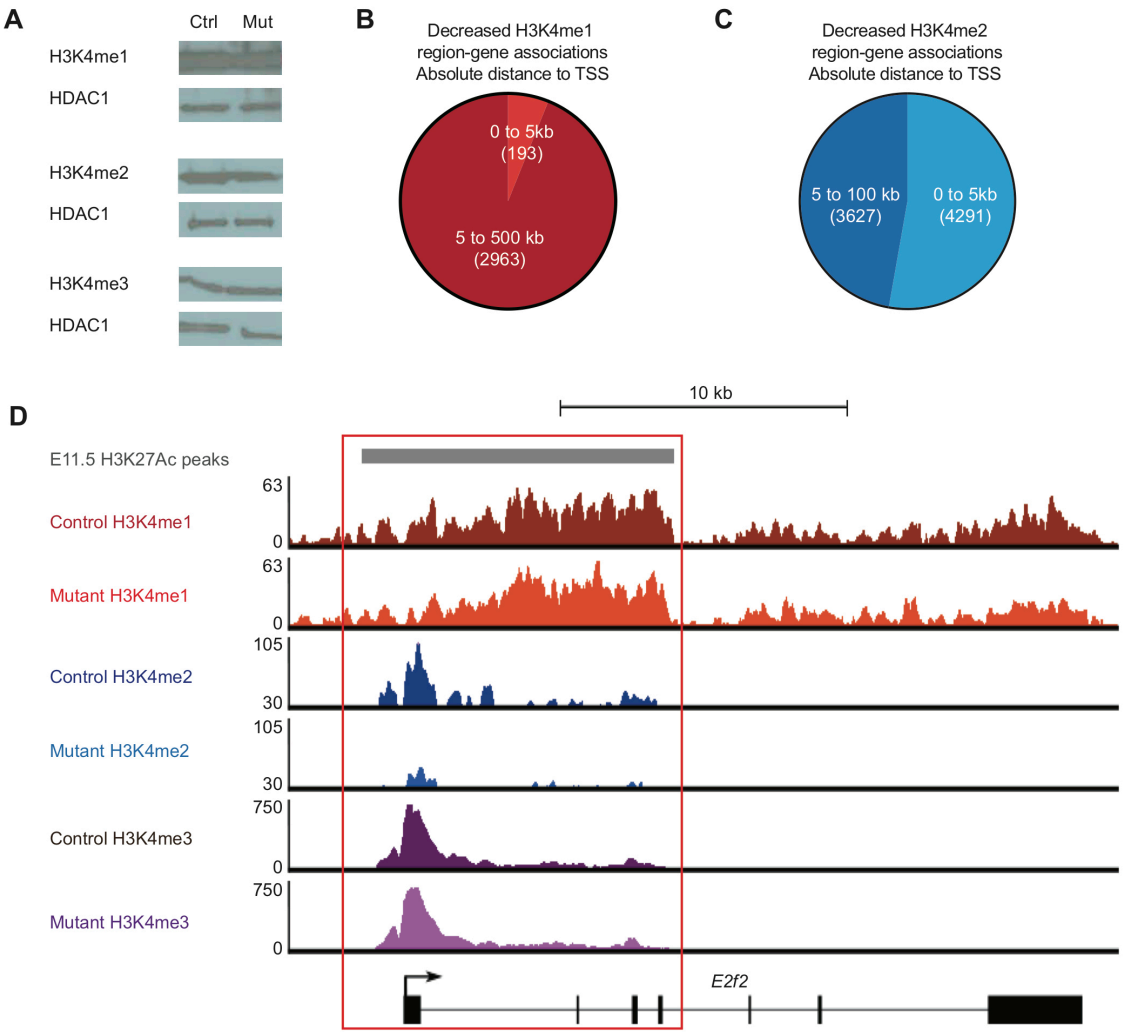


**Fig. S5. Myocardial deletion of *Kmt2d* results in a decrease in H3K4me1 levels at regions distinct from that with decreased H3K4me2 levels.**

(A) Western blot of H3K4me1, H3K4me2 and H3K4me3 bulk levels in E11.5 control *Tnnt2::Cre;Kmt2d*$^{fl/+}$ and *Tnnt2::Cre;Kmt2d*$^{fl/fl}$ hearts do not show obvious differences. HDAC1 is loading control.

(B) 2730 regions with decreased H3K4me1 levels (FDR<0.1) are assigned to 2473 genes by proximity within 100kb using Stanford GREAT. Decreased H3K4me1 region-gene associations are evaluated for absolute distance to TSS, showing that 193 region-gene associations are within 5 kb of TSS and 2963 region-gene associations are between 5 to 100 kb of TSS.

(C) 6417 regions with decreased H3K4me2 levels (FDR<0.1) are assigned to 6573 genes by proximity using Stanford GREAT. 3627 region-gene associations are within 5 kb of TSS and 4291 region-gene associations are between 5 to 100 kb of TSS.

(C) Venn diagram shows only 78 genes overlap between 2473 genes with decreased H3K4me1 levels and 492 genes downregulated in E11.5 *Tnnt2::Cre;Kmt2d*$^{fl/fl}$ hearts. GO categories of the subset of 78 genes are over-represented for ion transport and transcription regulation.

(D) Venn diagram representing overlap of 2730 regions with decreased H3K4me1 with 6699 regions with decreased H3K4me2. Of the overlapping 172 regions mapped to 186 genes, only 7 genes are downregulated in E11.5 *Tnnt2::Cre;Kmt2d*$^{fl/fl}$ hearts.

(E) Browser tracks showing average H3K4me1, H3K4me2 and H3K4me3 input normalized tag density at TSS of *E2f2*. Red box indicates region with decreased H3K4me2.

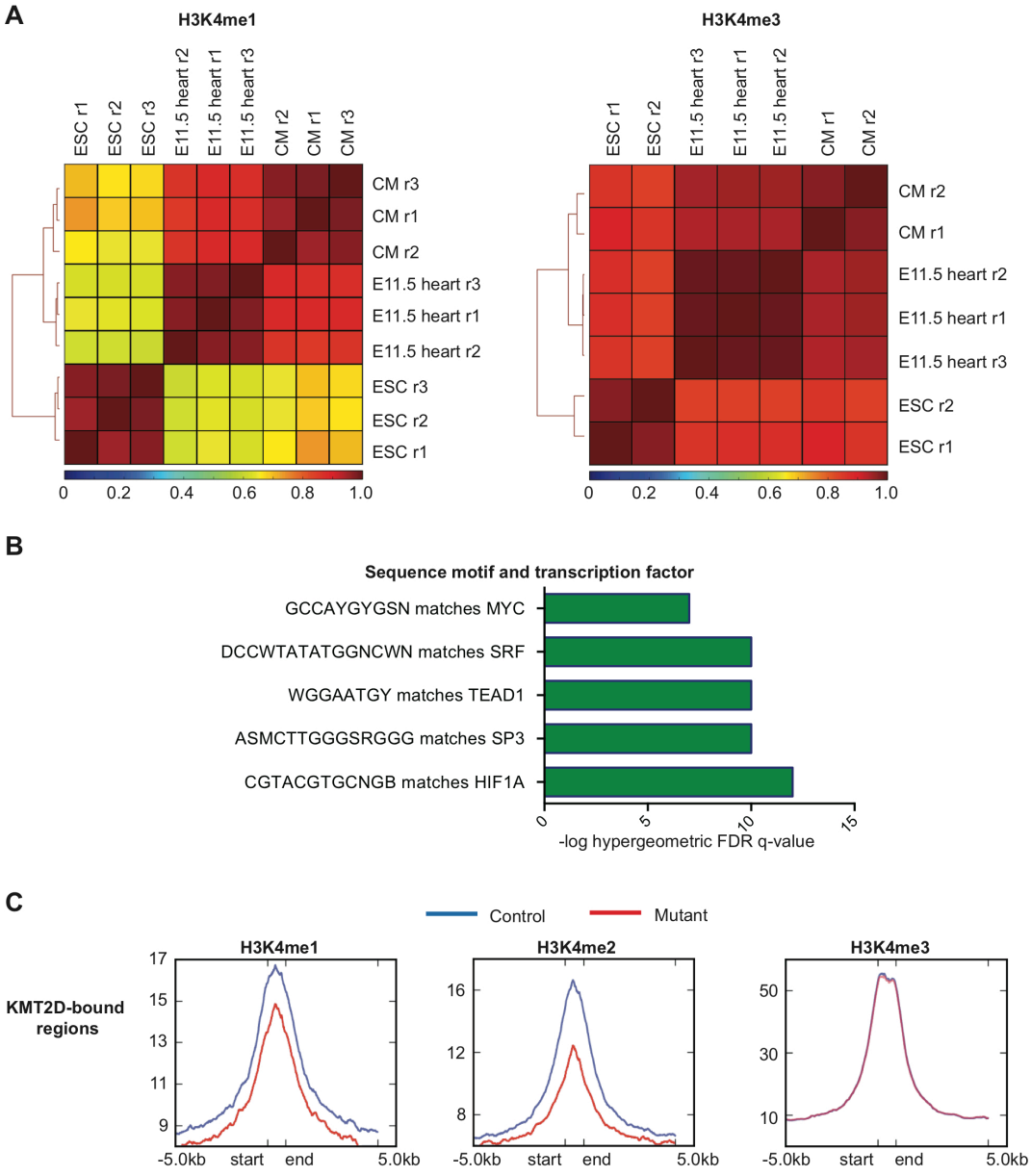


**Fig. S6. KMT2D binds to promoter and enhancer regions with motifs matching transcription factors important for heart development.**

(A) Spearman correlation of H3K4me1 and H3K4me3 ChIP-Seq data between embryonic stem cells (ESCs), derived cardiomyocytes (CM) (Wamstad et al., 2012) and E11.5 hearts show stronger correlation (red) of H3K4 methylation patterns between CM and E11.5 hearts, which are distinct from ESCs. r

represents replicate number and scale bar indicates Spearman correlation coefficient.

(B) Over-represented motifs found in KMT2D-bound regions match transcription factors important for heart development.

(C) Metagene profiles showing average distribution of H3K4me1, H3K4me2 and H3K4me3 input normalized tag density at KMT2D-bound regions sites in E11.5 control and *Tnnt2::Cre;Kmt2d*$^{fl/fl}$ hearts. Blue line denotes control hearts and red line denotes mutant hearts. Mutants show decreased H3K4me1 and H3K4me2 levels at KMT2D-bound regions, and no difference in H3K4me3 levels.

## (III) Supplementary Tables

**Table S1. Genotypes of offspring obtained from *Kmt2d* deletion by crossing *ACTB::Cre; Kmt2d*$^{\Delta/+}$ males with *ACTB::Cre; Kmt2d*$^{\Delta/+}$ females.**

| Deletion in tissue | Stage | Total animals | Heterozygotes | % heterozygotes | Null mutants | % null mutants |
|---|---|---|---|---|---|---|
| Global (*ACTB::Cre*) | E8.0 | 31 | 13 | 42 | 8 | 26 |
| | E8.5 | 9 | 5 | 56 | 0 | 0 |
| | E9.5 | 26 | 16 | 61 | 0 | 0 |
| | P0 | 21 | 9 | 43 | 0 | 0 |
| | P35 | 36 | 18 | 50 | 0 | 0 |

An additional 36 heterozygotes (*ACTB::Cre; Kmt2d*$^{\Delta/+}$) genotyped at P56 were obtained from crossing *ACTB::Cre* males with *Kmt2d*$^{fl/fl}$ females.

**Table S2. Genotypes of offspring obtained from conditional *Kmt2d* deletion using *Mesp1*$^{Cre}$, *Mef2cAHF::Cre, Tnnt2::Cre* or *Tie2::Cre*.**

| Deletion in tissue | Stage | Total animals | Mutants | % mutants |
|---|---|---|---|---|
| Mesodermal precursors (*Mesp1*$^{Cre}$) | E8.5 | 12 | 2 | 17 |
| | E9.0 | 17 | 4 | 24 |
| | E9.5 | 38 | 7 | 18 |
| | E10.5 | 15 | 0 | 0 |
| | E11.5 | 8 | 0 | 0 |
| | E12.5 | 5 | 0 | 0 |
| | P0 | 45 | 0 | 0 |
| Anterior heart field precursors (*Mef2cAHF::Cre*) | E9.5 | 14 | 4 | 29 |
| | E10.5 | 96 | 21 | 22 |
| | E11.5 | 40 | 8 | 20 |
| | E12.5 | 39 | 7 | 18 |
| | E13.5 | 14 | 0 | 0 |
| | P0 | 96 | 0 | 0 |
| Myocardial cells (*Tnnt2::Cre*) | E10.5 | 55 | 17 | 31 |
| | E11.5 | 414 | 104 | 25 |
| | E12.5 | 31 | 8 | 26 |
| | E13.5 | 19 | 5 | 26 |
| | E14.5 | 18 | 0 | 0 |
| | E16.5 | 6 | 0 | 0 |
| | P0 | 55 | 0 | 0 |

**Table S3.**

Click here to Download Table S3

**Table S4. Region-gene association distribution of H3K4me1 and H3K4me2 peaks.**

| Region-gene association | 0 to 5 kb | % of peaks in 0 to 5 kb | 50 to >500 kb | % of peaks in 50 to >500 kb |
|---|---|---|---|---|
| H3K4me1 | 35380 | 11.08% | 284003 | 88.92% |
| H3K4me2 | 34144 | 11.28% | 268429 | 88.72% |

**Table S5. Hypergeometric probability of downregulated genes with decreased H3K4 methylation associated with ion transport, compared to the population success of all downregulated genes associated with ion transport.**

| | | H3K4me1 | H3K4me2 |
|---|---|---|---|
| **Population size (P)** | All downregulated genes | 492 | 492 |
| **Number of successes in population (p)** | Downregulated genes associated with ion transport | 37 | 37 |
| **Ratio (p/P) in %** | Ratio of (Downregulated genes associated with ion transport / All downregulated genes) in % | 7.52% | 7.52% |
| **Sample size (S)** | All downregulated genes with decreased H3K4 methylation | 78 | 160 |
| **Number of successes in sample (s)** | Downregulated genes with decreased H3K4 methylation associated with ion transport | 8 | 18 |
| **Ratio (s/S) in %** | Ratio of (Downregulated genes with decreased H3K4 methylation associated with ion transport / All downregulated genes with decreased H3K4 methylation) in % | 10.25% | 11.25% |
| **Probability of drawing (number of s successes or more) in a sample of S, given (number of p successes) in population P** | Hypergeometric probability | 0.22 | 0.025 |

**Table S6. Hypergeometric probability of downregulated genes with decreased H3K4 methylation compared to the population success of all expressed genes with decreased H3K4 methylation.**

| | | H3K4me1 | H3K4me2 |
|---|---|---|---|
| **Population size (P)** | All expressed genes | 21664 | 21664 |
| **Number of successes in population (p)** | Expressed genes with decreased H3K4 methylation | 2778 | 6315 |
| **Ratio (p/P) in %** | Ratio of (Expressed genes with decreased H3K4 methylation/ All expressed genes) in % | 12.80% | 29.15% |
| **Sample size (S)** | All downregulated genes | 492 | 492 |
| **Number of successes in sample (s)** | Downregulated genes with decreased H3K4 methylation | 78 | 160 |
| **Ratio (s/S) in %** | Ratio of (Downregulated genes with decreased H3K4 methylation/ All downregulated genes) in % | 15.80% | 32.52% |
| **Probability of drawing (number of s successes or more) in a sample of S, given (number of p successes) in population P** | Hypergeometric probability | 0.027 | 0.054 |

**Table S7.**

Click here to Download Table S7

**Table S8. List of antibodies used in this study.**

| **Antibody** | **Company** | **Catalog No.** | **Host Isotype** | **Clone** | **Conjugate** |
|---|---|---|---|---|---|
| Anti-KMT2D | Sigma-Aldrich | HPA035977 | Rabbit IgG | N.A. | N.A. |
| Anti-KMT2D | Kai Ge lab (Lee et al., 2013) | N.A. | Rabbit IgG | N.A. | N.A. |
| Anti-ATP1A2 | Abcam | ab2871 | Mouse IgG1 | M7-PB-E9 | N.A. |
| Anti-HIF1A | Abcam | ab1 | Mouse IgG2b | H1alpha67 | N.A. |
| Anti-GFP | Abcam | ab13970 | Chicken IgY | N.A. | N.A. |
| Anti-TPM1 | DSHB | N.A. | Mouse IgG1 | CH-1 | N.A. |

| | | | | | |
|---|---|---|---|---|---|
| Anti-PECAM-1 | BD Pharmingen | 55370 | Rat IgG2a | N.A. | N.A. |
| Anti-HDAC1 | Abcam | ab7028 | Rabbit IgG | N.A. | N.A. |
| Anti-H3K4me1 | Diagenode | C15410194 | Rabbit IgG | pAb-194-050 | N.A. |
| Anti-H3K4me2 | Abcam | ab32356 | Rabbit IgG | Y47 | N.A. |
| Anti-H3K4me3 | Millipore | 07-473 | Rabbit IgG | N.A. | N.A. |
| Anti-Rabbit Secondary | Invitrogen | A-11037 | Goat | N.A. | Alexa 594 |
| Anti-Mouse Secondary | Invitrogen | A-11032 | Goat | N.A. | Alexa 594 |
| Anti-Rat Secondary | Invitrogen | A-11007 | Goat | N.A. | Alexa 594 |
| Anti-Chicken Secondary | Invitrogen | A-11039 | Goat | N.A. | Alexa 488 |

**Table S9. List of primers used in this study.**

| **Gene** | **F/R** | **Sequence** |
|---|---|---|
| *Kmt2d* floxed allele (genotyping) | F | ATTGCATCAGGCAAATCAGC |
| | R | GCAGAAGCCTGCTATGTCCA |
| *Kmt2d* null allele (genotyping) | F | GTTCACTCAGTGGGGCTGTG |
| | R | GCAGAAGCCTGCTATGTCCA |
| *Kmt2d* exon 16-17 (qPCR) | F | GACCTGCTAATCCAGTGTCG |
| | R | CTGCTCCACCTCATCCTCTG |
| *Actb* (qPCR) | F | GCTCTTTTCCAGCCTTCCTT |
| | R | TGGCATAGAGGTCTTTACGGA |
| *Atp1a2* (qPCR) | F | CTTTGGCTGCCTTTCTGTCT |
| | R | AGCTTCCGAACTTCATCATAGAT |
| *Atp2b4* (qPCR) | F | CTGACCATGGAGCAGTGGAT |
| | R | GGAACTTCAGAGACTTGGTAGG |
| *Cacna1h* (qPCR) | F | GTGAGCCTCTCTGCCATCC |
| | R | TGTCCAGCAGCAGTGTGAC |
| *Camk2a* (qPCR) | F | ATCAAAGTGACAGAGCAGCT |
| | R | CCTCTGGTTCAAAGGCTGTC |
| *Casq1* (qPCR) | F | GGAATCCACATTGTCGCCTT |
| | R | CGGGGTTCTCAGTGTTGTCT |
| *Cox6a2* (qPCR) | F | GCCCAGAGTTCATCCCGTAT |
| | R | GATTGACGTGGGGATTGTGG |
| *Eln* (qPCR) | F | CTGGTGGAGTTGGCCCTG |
| | R | TTAGCAGCAGATTTAGCGGC |

| | | |
|---|---|---|
| *Fxyd1* (qPCR) | F | CCGACGAAGAGGAGGGAAC |
| | R | CTGGCTGAGTTTCCTGGAGT |
| *Rgs5* (qPCR) | F | TCCCTGGACAAGCTTCTCC |
| | R | GGCAACCCAGAACTCAAGGT |
| *Snta1* (qPCR) | F | TGTCATCGGGCTGCTGAA |
| | R | GTGAAGCCCTTGTCGATGTG |

**(IV) Supplementary references**

**Landt, S. G., Marinov, G. K., Kundaje, A., Kheradpour, P., Pauli, F., Batzoglou, S., Bernstein, B. E., Bickel, P., Brown, J. B., Cayting, P., et al.** (2012). ChIP-seq guidelines and practices of the ENCODE and modENCODE consortia. *Genome Res* **22**, 1813–31.

**Langmead, B. and Salzberg, S. L.** (2012). Fast gapped-read alignment with Bowtie 2. *Nat Methods* **9**, 357–9.

**Li, H., Handsaker, B., Wysoker, A., Fennell, T., Ruan, J., Homer, N., Marth, G., Abecasis, G., Durbin, R. and Subgroup, 1000 Genome Project Data Processing** (2009). The Sequence Alignment/Map format and SAMtools. *Bioinformatics* **25**, 2078–2079.

**McLean, C. Y., Bristor, D., Hiller, M., Clarke, S. L., Schaar, B. T., Lowe, C. B., Wenger, A. M. and Bejerano, G.** (2010). GREAT improves functional interpretation of cis-regulatory regions. *Nat Biotechnol* **28**, 495–501.

**Neph, S., Vierstra, J., Stergachis, A. B., Reynolds, A. P., Haugen, E., Vernot, B., Thurman, R. E., John, S., Sandstrom, R., Johnson, A. K., et al.** (2012). An expansive human regulatory lexicon encoded in transcription factor footprints. *Nature* **489**, 83–90.

**Ramírez, F., Dündar, F., Diehl, S., Grüning, B.A., and Manke, T.** (2014). deepTools: a flexible platform for exploring deep-sequencing data. *Nucleic Acids Res* **42**, W187-89.